ACCOUNTS of chemical research

Subscriber access provided by American Chemical Society

Article

Direct Observation of Amyloid Fibril Growth, Propagation, and Adaptation

Tadato Ban, Keiichi Yamaguchi, and Yuji Goto

Acc. Chem. Res., **2006**, 39 (9), 663-670• DOI: 10.1021/ar050074l • Publication Date (Web): 28 July 2006

Downloaded from http://pubs.acs.org on March 2, 2009

More About This Article

Additional resources and features associated with this article are available within the HTML version:

- Supporting Information
- Links to the 6 articles that cite this article, as of the time of this article download
- Access to high resolution figures
- Links to articles and content related to this article
- Copyright permission to reproduce figures and/or text from this article

View the Full Text HTML

ACS Publications
High quality. High impact.

Accounts of Chemical Research is published by the American Chemical Society. 1155 Sixteenth Street N.W., Washington, DC 20036

Direct Observation of Amyloid Fibril Growth, Propagation, and Adaptation

TADATO BAN, KEIICHI YAMAGUCHI, AND YUJI GOTO*

Institute for Protein Research, Osaka University, and CREST, Japan Science and Technology Agency, Suita, Osaka 565-0871, Japan

Received February 27, 2006

ABSTRACT

Amyloid fibrils form through nucleation and growth. To clarify the mechanism involved, direct observations of both processes are important. First, seed-dependent fibril growth of β2-microglobulin (β2-m) and amyloid β peptide was visualized in real time at the single fibril level using total internal reflection fluorescence microscopy combined with the binding of thioflavin T, an amyloid-specific fluorescence dye. Second, using atomic force microscopy, ultrasonication-induced formation of β2-m fibrils was shown, indicating that ultrasonication is useful to accelerate the nucleation process. Third, with the proteolytic fragment of β2-m, propagation and a transformation of fibril morphology was demonstrated. These direct observations indicate that template-dependent growth and structural diversity are key factors determining the structure and function of amyloid fibrils.

1. Introduction

Amyloid fibrils have been a critical subject in recent studies of proteins since they were recognized to be associated with the pathology of more than 20 serious human diseases.[1−3] Although no sequence or structural similarity has been found among the amyloid precursor proteins, amyloid fibrils share several common structural and spectroscopic properties. Irrespective of protein species, electron microscopy (EM) and X-ray fiber diffraction indicate that amyloid fibrils are relatively rigid and straight with a diameter of 10−15 nm and several layers of cross-β sheets. Amyloid fibrils form via a nucleation-dependent process in which non-native forms of precursor proteins or peptides slowly associate to form a nucleus, which is followed by an extension reaction, where the nucleus grows by the sequential incorporation of precursor molecules.[1−5] Structural studies using solid-state NMR have shown that amyloid fibrils are stabilized by juxtaposing hydrophobic segments minimizing electrostatic repulsion.[6,7] From the hydrogen/deuterium exchange of amide protons, amyloid fibrils are shown to be stabilized by an extensive network of hydrogen bonds substantiating β-sheets.[8,9] On the basis of various approaches, increasingly convincing structural models of amyloid fibrils are emerging.

The heterogeneity of amyloid fibrils has been a focus recently. It has been shown that amyloid β (Aβ) amyloid fibrils with different morphological features have different underlying side-chain structures as revealed by solid-state NMR measurements and that both the morphology and the molecular structure are self-propagated by seeding.[7] A similar observation of the template-dependent propagation of distinct fibrils was made with insulin.[10] More recently, mammalian prion amyloids from different species were shown to differ distinctly in secondary structure and morphology as measured by Fourier transform infrared (FTIR) and atomic force microscopy (AFM), respectively.[11] Importantly, cross-seeding of prion monomers from one species with preformed fibrils from another species produced a new amyloid strain that inherited the secondary structure and morphology of the template fibrils. Strain-specific conformational differences were also found for yeast Sup35 prion amyloid fibrils.[12] These findings may explain the structural basis underlying conformational memory as suggested for prion diseases.[13−15]

To obtain further insight into the structure and heterogeneity of amyloid fibrils, direct observation of individual fibrils is important. Here, we characterize each process of nucleation, growth, propagation, and adaptation by direct observation at the single fibrillar level. On the basis of these observations, we propose free energy landscapes illustrating the formation, stability, and transformation of amyloid fibrils.

2. Seed-Dependent Amyloid Fibril Growth

Dialysis-related amyloidosis is a serious problem among patients who have been receiving hemodialysis for more than 10 years.[16,17] It is caused by the deposition of amyloid fibrils of β2-microglobulin (β2-m) in the synovia of the carpal tunnel. In its native state, β2-m adopts a typical immunoglobulin fold, consisting of seven β-strands and one intrachain disulfide bond[18] (Figure 1a). In patients suffering from dialysis-related amyloidosis, β2-m is converted into the amyloid fibrils, as usually seen in other amyloidoses. Although an increase in the concentration of β2-m in blood over a long period is the most important risk factor for amyloidosis, the molecular mechanism involved remains unclear.

Because of its suitable protein size useful for various physicochemical approaches and relatively simple characteristics revealed in *in vitro* analyses, β2-m is becoming a target of extensive study for addressing the mechanism by which amyloid fibrils form.[19−24] β2-m can be converted to amyloid fibrils *in vitro* under acidic conditions through

Tadato Ban received a Ph.D. (2005) of Polymer Sciences from Osaka University. He is a postdoctoral researcher studying amyloid fibrils using total internal reflection fluorescence microscopy.

Keiichi Yamaguchi is a Ph.D. candidate studying the mechanism of amyloid fibril formation and propagation.

Yuji Goto received a Ph.D. (1982) of Biochemistry from Osaka University. He visited U.C. Santa Cruz as a postdoctoral fellow (1986−1988). He joined the Institute for Protein Research as a Professor in 1998. His research interests include protein folding and misfolding.

* Corresponding author. E-mail address: ygoto@protein.osaka-u.ac.jp.

10.1021/ar050074l CCC: $33.50 © 2006 American Chemical Society
Published on Web 07/28/2006

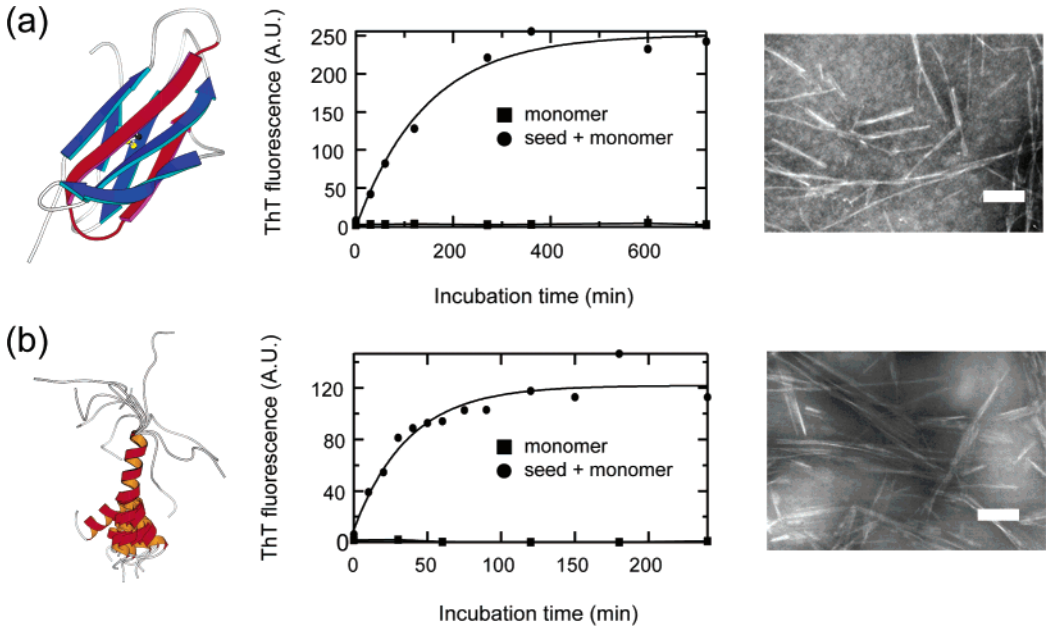

FIGURE 1. Formation of amyloid fibrils of β2-m (a) and Aβ(1−40) (b). In panel a, a three-dimensional representation of monomeric β2-m in the native state (PDB entry 1HSB) is shown on the left. The location of the K3 peptide is indicated in red. The time course of seed-dependent growth of amyloid fibrils of β2-m at pH 2.5 as monitored by the increase in ThT fluorescence is presented in the center. The standard conditions described in ref 30 were used. Electron microscopic images of β2-m fibrils obtained by the seed-dependent extension are shown on the right. In panel b, a three-dimensional representation of monomeric Aβ(1−40) in a water-micelle environment (PDB entry 1BA4) is shown on the left. The time course of seed-dependent growth of amyloid fibrils of Aβ(1−40) at pH 7.5 is presented in the center. Electron microscopic images of Aβ(1−40) fibrils prepared by the seed-dependent extension are shown on the right. Adapted from ref 26 with permission. The three-dimensional representation was drawn by MOLSCRIPT.[42] Scale bars represent 200 nm.

seed-dependent fibril growth using seed fibrils originally purified from patients[4] (Figure 1a). Although acidic fibrils are different from the fibrils in patients formed at neutral pH, they have a fairly homogeneous needle-like morphology, which is an advantage when analyzing the biochemical and biophysical properties of β2-m amyloid fibrils. Seed-dependent fibril growth was also established for Aβ(1−40) under physiological conditions at pH 7.5 (Figure 1b).[5]

3. Total Internal Reflection Fluorescence Microscopy

We developed a new technique for the direct observation of amyloid fibrils using total internal reflection fluorescence microscopy (TIRFM) combined with thioflavin T (ThT) fluorescence (Figure 2).[25,26] TIRFM has been useful for monitoring single molecules by effectively reducing the background fluorescence under the evanescent field formed on the surface of a quartz slide.[27−29] When a laser is incident on the interface between a quartz slide (high reflection index) and an aqueous solution (low reflection index) at the critical angle for total internal reflection, the evanescent field is produced beyond the interface in the solution. Because the evanescent field is produced with a penetration depth of about 150 nm, the illumination is restricted to fluorophores either bound to the quartz slide surface or located close by, resulting in highly reduced background fluorescence. Furthermore, with the careful selection of optical elements, the background fluorescence can be reduced by 2000-fold compared with ordinary epi-

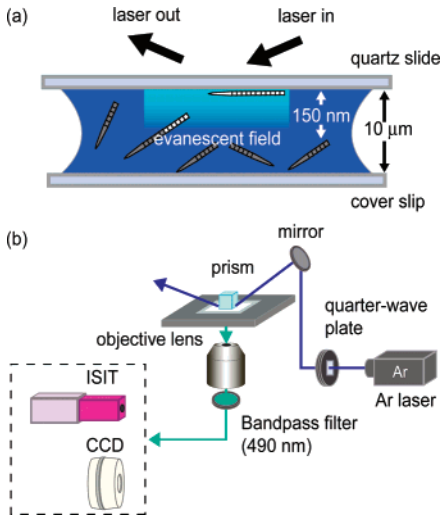

FIGURE 2. Schematic representation of amyloid fibrils revealed by total internal reflection fluorescence microscopy. In panel a, the penetration depth of the evanescent field formed by the total internal reflection of laser light is ∼150 nm for a laser light at 455 nm, so only amyloid fibrils lying in parallel with the slide glass surface were observed. Panel b shows a schematic diagram of a prism-type TIRFM system on an inverted microscope. ISIT denotes image-intensifier-coupled silicone intensified target camera; CCD denotes charge-coupled device camera.

fluorescence microscopy. On the other hand, ThT is a reagent known to become strongly fluorescent upon binding to amyloid fibrils,[30] so one can detect the fibrils specifically without covalent modification. Importantly, because the evanescent field formed by the total internal

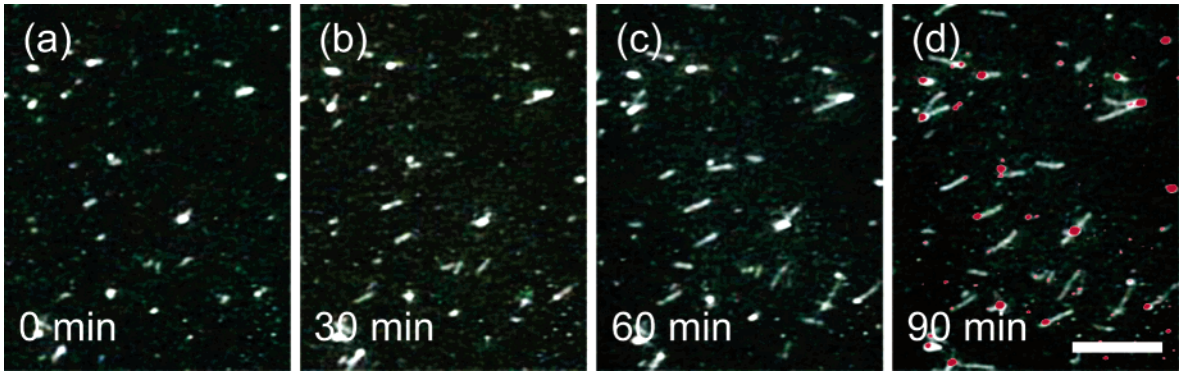

FIGURE 3. Direct observation of β2-m amyloid fibril growth obtained by TIRFM. Adapted from ref 25 with permission. Incubation times are 0, 30, 60, and 90 min. The scale bars are 10 μm. In panel d, ThT fluorescence at 0 min was overlaid in red to identify the locations of seed fibrils.

reflection of laser light penetrates to a depth of 150 nm, one can selectively monitor fibrils lying along the slide glass within 150 nm and so can obtain the exact length of the fibrils. By a combination of amyloid fibril-specific ThT fluorescence and TIRFM, it would be possible to observe the amyloid fibrils and the process by which they form without introducing any fluorescence reagent covalently bound to the protein molecule.[25,26]

4. Real-Time Observation of Fibril Growth

Real-time observation of the growth of individual β2-m fibrils was carried out on the surface of quartz slides (Figure 3).[25] At time zero, the β2-m seeds appeared as bright fluorescent spots. Then, fibril growth occurred from the seed fibrils, with saturation occurring in a couple of hours when the monomeric β2-m was depleted. The overall time course of fibril growth was similar to that in solution with similar concentrations of seeds and monomers. Intriguingly, most of the fibrils showed unidirectional growth starting from one end of the seeds. Although we cannot exclude the possibility that the interaction with the glass surface was responsible for the unidirectional extension, the unidirectional picture is likely to hold for the formation of fibrils of β2-m and also of Aβ(1−40) (see below).

This approach using ThT can be applied to various amyloid fibrils since the binding of ThT is common to amyloid fibrils. This was demonstrated with Aβ(1−40) amyloid fibrils,[26] revealing more dramatic images since we could perform the experiments at pH 7.5, where the fluorescence of ThT is much stronger than that at pH 2.5 (Figure 4). The growth of fibrils occurred concomitantly at many seeds. Although several fibrils often developed from apparently one seed, it is likely that clustered seeds produced such a radial pattern. Once started, unidirectional growth continued producing remarkably long fibrils more than 15 μm in length. Considering that TIRFM selectively monitors fibrils lying along the slide within 150 nm, the interaction of fibrils with the quartz surface caused the lateral growth. In addition, the combination of relatively rapid fibril growth and less aggregation of fibrils weakly fixed on the quartz surface enabled the formation of remarkably long fibrils.

Intriguingly, we occasionally observed growth to be aligned in a similar direction, for example, vertically aligned growth (Figure 5a), implying that the interaction with an ordered quartz surface significantly affected the direction of growth. We sometimes observed a swinging motion of the growing head resulting in a shift in the direction of growth consequently producing rugged fibrils (Figure 5c). Notably, a dramatic swinging motion was occasionally observed, suggesting that the fibrils are flexible, bending both horizontal and vertical to the plane of the quartz surface (Figure 5d). In addition, real-time observation revealed important images suggesting a transient loss of cooperativity in fibril growth (Figure 5b). After the cooperative growth with a blunt end (images from 6 to 10 min), the end frayed into three thinner filaments (image at 12 min). In the next step, braiding of the three filaments recovered the blunt end (image at 14 min), implying that the mature fibril is made of three protofilaments.

The remarkable length of the fibrils enabled an exact analysis of the rate of growth of individual fibrils. The growth at the early and middle stages seems to occur in an all-or-none manner: when the fibril extends, the rate is almost constant (~0.3 μm/min) independent of fibril species. There were cases where the growth paused briefly, possibly because of physical obstacles or local depletion of monomers. When the growth restarted, however, a similar rate of 0.3 μm/min was regained. Similar discontinuous growth, termed the stop-and-run mechanism, was also observed during the growth of α-synuclein protofibrils monitored by AFM *in situ*.[31]

5. Ultrasonication-Induced Formation of Fibrils

The formation of amyloid fibrils under our quiescent conditions occurred only in the presence of seed fibrils (Figure 1). However, it has been reported that the agitation of a solution by shaking or stirring under acidic conditions induced the formation of fibrils.[32] We found that the ultrasonication of a monomeric β2-m solution also results in the formation of fibrils (Figure 6).[33] The same conditions as used for the standard seed-dependent reaction (i.e., 25 μM β2-m monomer in 50 mM glycine−HCl buffer (pH 2.5) containing 100 mM NaCl) were used to examine the

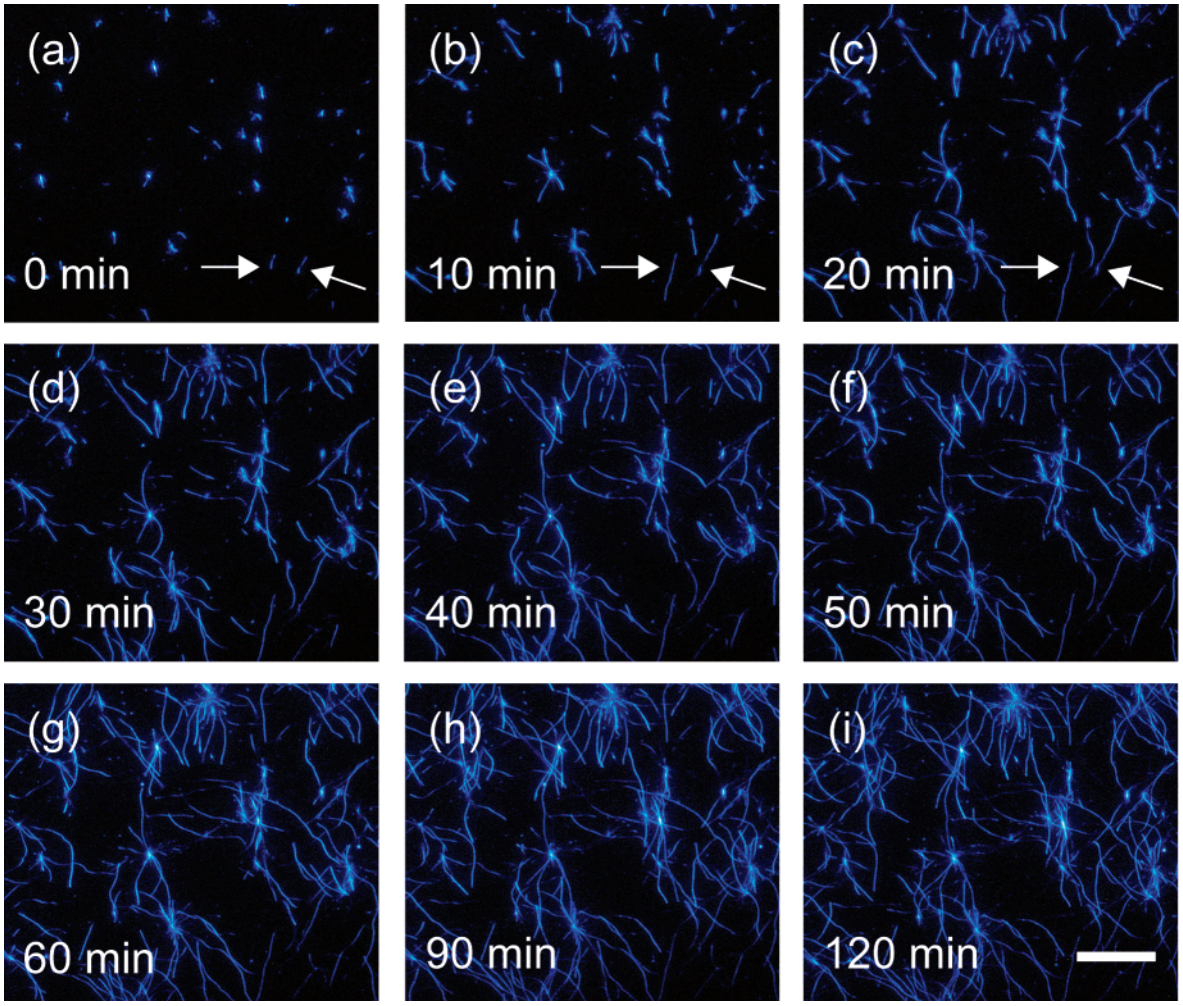

FIGURE 4. Direct observation of Aβ(1−40) amyloid fibril growth by TIRFM: (a−i) real-time monitoring of fibril growth on glass slides. Arrows indicate the unidirectional growth of Aβ from a single seed fibril. The scale bar represents 10 μm. Adapted from ref 26 with permission.

effects of ultrasonication. After preparation of the reaction mixture in an Eppendorf tube on ice, ultrasonic treatment was started with the tube placed in a water bath at 37 °C. Repeated ultrasonication for 1 min in every 10 min induced, after a lag-time of about 1 h, a sudden and remarkable increase in ThT fluorescence (Figure 6a). The ThT fluorescence value (∼300) was much larger than that (∼200) of the standard seed-dependent reaction. AFM images of the solution at 3 h revealed substantial numbers of short fibrils (10−40 nm) about 3 nm in height (Figure 6b,d).

The seed-dependent extension of fibrils was examined at pH 2.5 using the sonication-induced short fibrils (i.e., the first generation of fibrils, F1) as seeds (Figure 6a). It should be noted that the reaction was carried out *without sonication*. The ThT fluorescence increased dramatically without a lag-phase. AFM images revealed the formation of long and straight fibrils with a diameter of 3 nm (Figure 6c,e). The result demonstrates that the short F1 fibrils formed by sonication acted as seeds for subsequent growth, producing the second generation of fibrils (F2), a phenomenon characteristic of amyloid fibrils. The repeated seeding reactions produced the third and fourth generations of fibrils (F3 and F4, respectively) with essentially the same kinetics as the F2 fibrils and with the same morphology measured by AFM. Compared with the fibrils generated by the standard reaction with seeds originally from patients (Figure 6f), sonication-induced fibrils were thin, suggesting that they correspond to the protofibrils of mature fibrils.

6. Inheritance *versus* Adaptation of Fibril Conformation

In many amyloidogenic proteins, short peptides called minimal or essential sequences can form amyloid fibrils by themselves.[34] A 22-residue K3 peptide, Ser20−Lys41, obtained by digestion of β2-m with *Acromobacter* protease I, forms amyloid-like fibrils in various solutions.[35,36] It has been reported that alcohols, in particular trifluoroethanol (TFE), induce peptides to form amyloid-like fibrils.[37,38] K3 peptide also formed amyloid-like fibrils at low concentrations of TFE in 10 mM HCl (pH ∼2), as confirmed by the AFM measurements (Figures 7 and 8).[39,40]

An examination of TFE-induced fibrils by CD revealed the presence of two types in 20% (v/v) TFE and 10 mM HCl, depending on the method of preparation.[40] When lyophilized K3 peptide was dissolved in 10 mM NaOH and

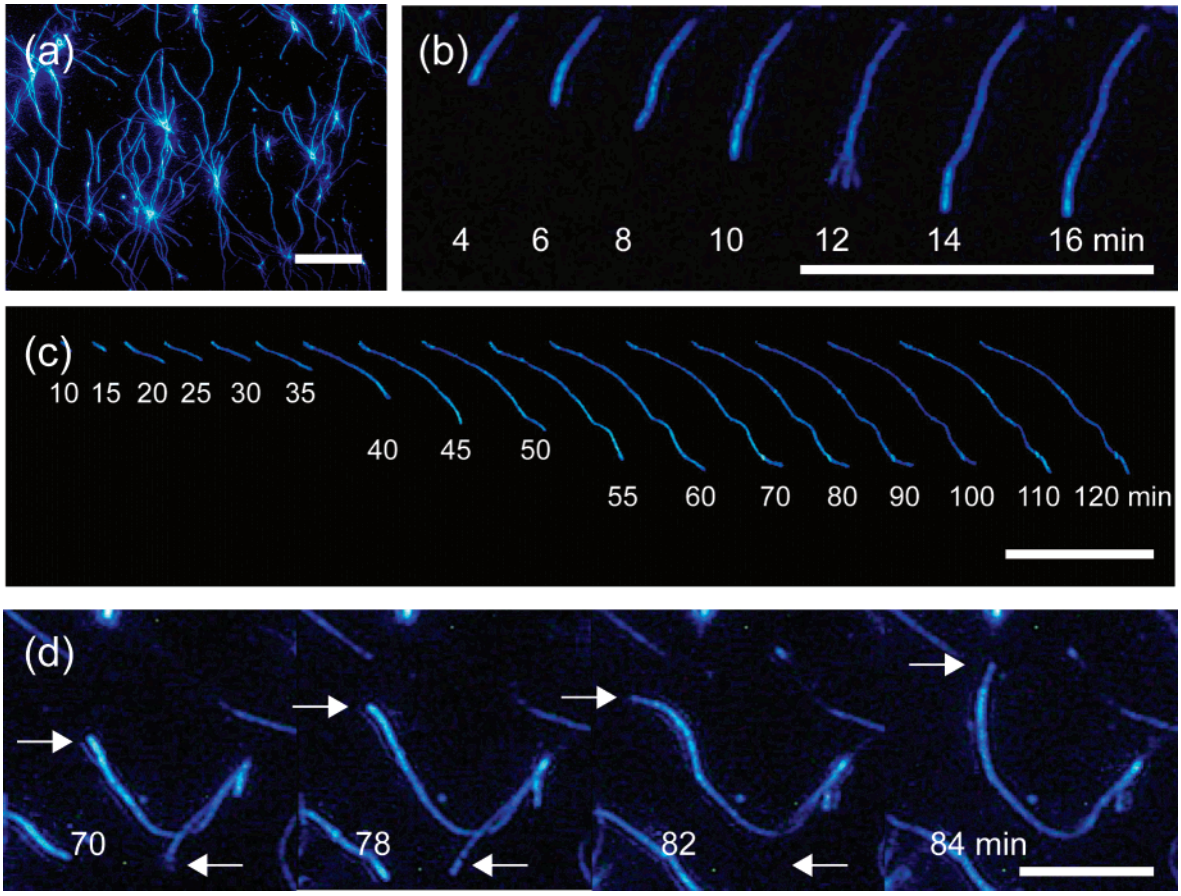

FIGURE 5. Characteristic images of Aβ(1−40) amyloid fibril growth revealed by TIRFM: (a) vertically aligned image of fibrils; (b) growth with transient fraying of the growing end at 12 min; (c) growth with a swinging head producing a rugged fibril. The scale bars in panels a−c are 10 μm. Panel d shows growth with flexible bending motion. Top and bottom arrows indicate the bending horizontal and vertical, respectively, to the plane of the quartz surface. The scale bar represents 5 μm. Images in panels a−c are adapted from ref 26 with permission.

then diluted with 20% (v/v) TFE and 10 mM HCl, K3 peptide formed fibrils exhibiting a unique CD spectrum with a minimum around 210 nm and immensely large negative ellipticity (−40 600 deg cm^{-2} mol^{-1}), suggesting the formation of a highly ordered β-sheet structure (Figure 7). This spontaneous formation of fibrils was accompanied by a lag phase of about 3 h. On the other hand, dissolving K3 peptide directly into 20% (v/v) TFE and 10 mM HCl produced fibrils with a standard CD spectrum for a β-sheet-rich conformation: a moderate minimum (−16 100 deg cm^{-2} mol^{-1}) at 218 nm (Figure 8). Importantly, this process proceeded without a lag phase, implying the presence of oligomers or undissolved aggregates that act as seeds. Here, the fibrils with an extremely large minimum at 210 nm and a moderate minimum at 218 nm are referred to as "f210" and "f218" fibrils, respectively.

Taking advantage of the lag time of 3 h for the monomeric K3 peptide originally dissolved in 10 mM NaOH, we could study the effects of seeding. The two types of seed fibrils were added to the 10 mM NaOH-dissolved monomeric K3 in 20% (v/v) TFE and 10 mM HCl. When f210 seeds (S0) were used, f210 fibrils (F1) were reproduced without a lag phase (Figure 7). Similarly, when the f218 seeds (S0) were used, f218 fibrils (F1) were reproduced without a lag phase (Figure 8). However, a slight shift of the minimum to a lower wavelength as well as a slight increase in intensity was noted. Thus, we repeated the seeding reaction carefully and found that the f218 fibrils transformed gradually into f210 fibrils. After several cycles of seeding, the CD spectrum of the transformed fibrils was indistinguishable from that of f210 fibrils, indicating the conformational adaptation.

The two types of K3 fibrils showed a marked difference in morphology when examined by AFM. The f210 fibrils were thin with a diameter of 2.3 ± 0.4 nm and were untwisted. They were quite long and remarkably homogeneous. The f210 fibrils (F1) produced by seeding were also thin (2.1 ± 0.3 nm) and long, the same as the seeds (F0). Further seeding did not change the morphology of f210 fibrils. In contrast, the f218 fibrils (F0) were relatively thick with diameters of 1.8−9.0 nm and shorter in length. The f218 fibrils (F1) formed by seeding were also thick with a diameter of 1.6−8.5 nm. Notably, a small number of thin fibrils ~2 nm in diameter were seen among the thick fibrils, suggesting the concomitant formation of f210 fibrils. After the second cycle of seeding (F2), the population of thin filaments increased significantly. After five cycles of seeding (F5), the AFM image was indistinguishable from that of the f210 fibrils, indicating that the f218 fibrils are transformed completely into f210 fibrils. The results indicate that, although two types of fibrils can coexist in 20% (v/v) TFE and 10 mM HCl, the seed-

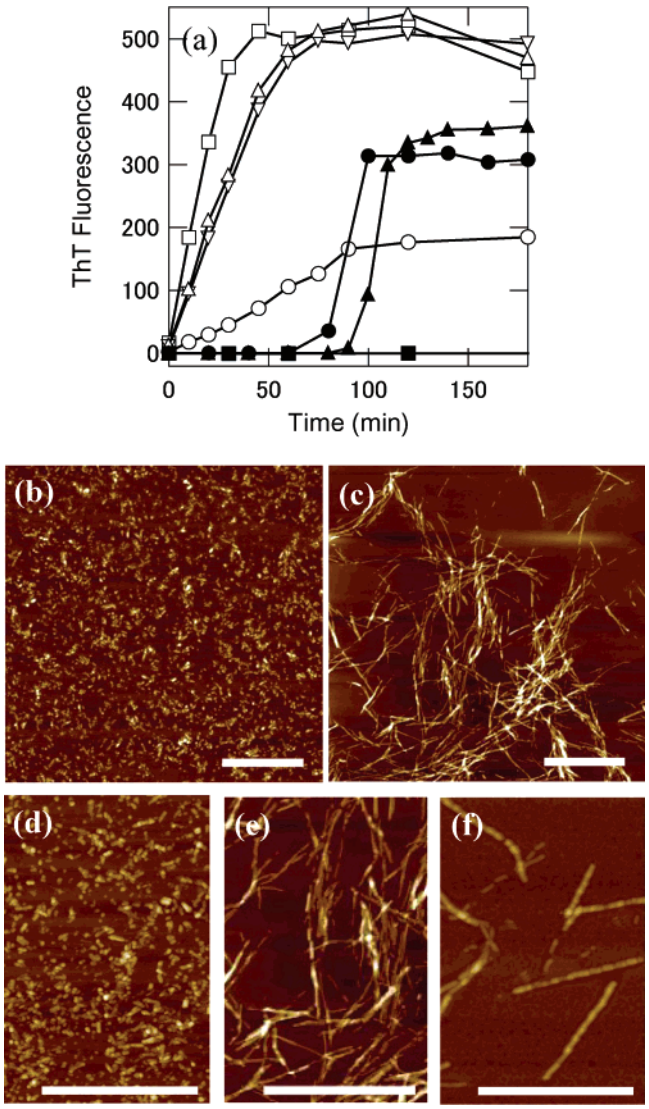

FIGURE 6. Ultrasonication-induced formation of β2-m fibrils at pH 2.5. Panel a shows kinetics monitored by ThT fluorescence. Closed symbols (●, ▲) represent ultrasonication-induced formation of the F1 fibril exhibiting a lag time (60−120 min). The results of two independent experiments are shown, indicating a slight variation of lag time. Open symbols (□, Δ, ▽) represent the extension reactions producing F2 (□), F3 (Δ), and F4 (▽) fibrils, in which ultrasonication-induced F1, F2, and F3 fibrils were used as seeds, respectively. Open circles (○) represent a standard fibril extension reaction with seeds of originally *ex vivo* β2-m amyloid fibrils. Closed squares (■) represent the control reaction without seeds and ultrasonication. Panels b−f show AFM images of F1 (b, d) and F2 (c, e) fibrils and fibrils extended by the standard reaction at pH 2.5 (f). The scale bars represent 1 μm. Adapted from ref 33 with permission.

dependent growth favors the formation of f210 fibrils over f218 fibrils.

A similar phenomenon of adaptation was observed for the formation of amyloid fibrils of β2-m at pH 7.0, where repeated self-seeding causes a marked acceleration of growth after a couple of cycles.[41] Seeding-dependent adaptation can be explained by the competitive propagation of different types of fibrils with different growth rates. If this is also the case of the observed adaptation of f218 fibrils to f210 fibrils, a tiny fraction of f210 fibrils present

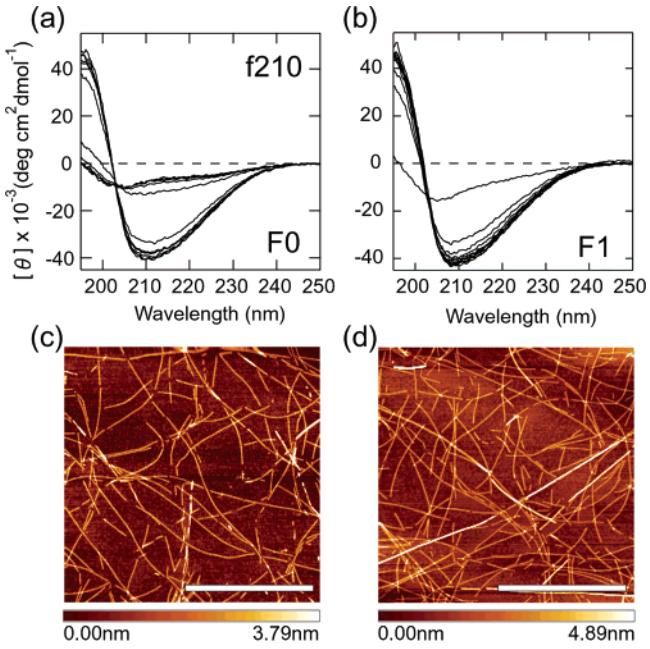

FIGURE 7. Seeding-dependent propagation of f210 fibrils: (a, b) CD spectra of f210 fibrils prepared by spontaneous polymerization (F0) (a) and by seeding of f210 fibrils (F1) (b) in 20% (v/v) TFE and 10 mM HCl at 25 °C; (c, d) AFM images of F0 (c) and F1 (d) f210 fibrils. Adapted from ref 40 with permission.

in the preparation of f218 fibrils might be propagated more rapidly than f218 fibrils during the cycles of self-seeding. Indeed, simulated kinetics of the repeated seeding experiments with f218 seeds reproduced the observed kinetics monitored by CD, indicating the validity of the competitive propagation model.

7. Free Energy Landscapes Illustrating Fibril Formation, Propagation, and Adaptation

Free energy diagrams will be useful for considering the direct observations of amyloid fibrils as described here (Figure 9). The amyloidogenic fragment of β2-m forms two types of fibrils differing significantly in secondary and tertiary structures and morphology. The two fibrils can be inherited by a template-dependent propagation, suggesting the structural basis underlying conformational memory as proposed for prion diseases.[11−15] On the other hand, we observed an adaptation in which repeated seeding gradually transforms one type of fibril to the other; thus the conformational memory is lost. This inheritance and adaptation of amyloid fibrils can be explained by free energy diagrams with two minima (Figure 9).

We consider that conformational inheritance and adaptation are complementary phenomena both manifesting the principles of amyloid fibril architecture. Whether inheritance or adaptation occurs depends on the nature of amyloidogenic proteins and solvent conditions. We propose that one important factor is the rates of template-dependent growth of different fibrils. Under conditions where the spontaneous formation of fibrils is difficult (routes a) and only one type of seed is present (either of routes b), the inheritance of a unique fibril conformation

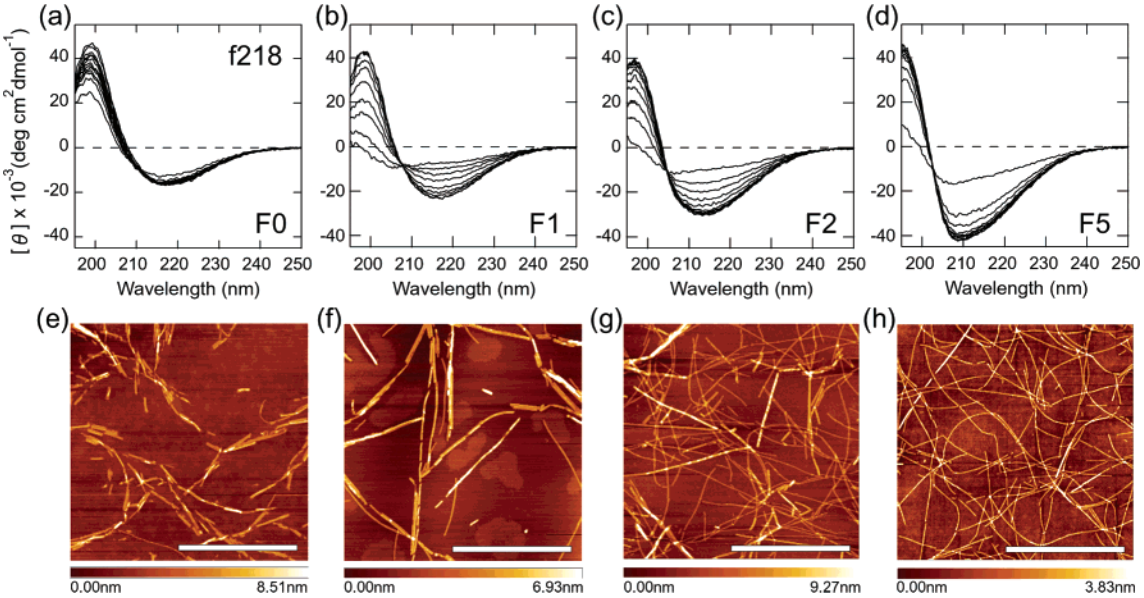

FIGURE 8. Transformation of f218 fibrils into f210 fibrils during the repeated cycles of self-seeding: (a−d) seed-dependent formation of fibrils in 20% (v/v) TFE and 10 mM HCl at 25 °C monitored by CD—types of fibrils made were F0 (a), F1 (b), F2 (c), and F5 (d); (e−f) AFM images of F0 (e), F1 (f), F2 (g), and F5 (h) fibrils. Adapted from ref 40 with permission.

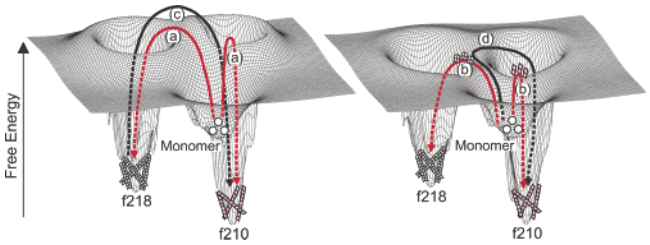

FIGURE 9. Schematic representation of energy landscapes for the formation of f210 and f218 fibrils in the absence (left) and presence (right) of seeds: (a) spontaneous formation of f210 and f218 fibrils with a high free energy barrier; (b) seed-dependent formation of f210 and f218 fibrils with a reduced free energy barrier. Starting with f218 fibrils contaminated with a small amount of f210 fibrils, the repeated-seeding reaction increases the population of f210 fibrils leading to conformational adaptation. Trace c represents conformational adaptation by the direct conversion of f218 fibrils to f210 fibrils through the free energy barrier separating them. The conversion can also occur through the monomers in equilibrium with the two types of amyloid fibrils. Trace d represents conformational adaptation during the growth of single fibrils, where f218 seeds are used to initiate the reaction but the peptides assume a thermodynamically stable f210 conformation.

would continue as argued for prion diseases. In contrast, adaptation to thermodynamically more stable fibrils as observed here can be explained by a competitive propagation mechanism (route b). It is likely that adaptation plays a role during the development of amyloidosis.

Additionally, the free energy diagram suggests that the conformation of amyloid fibrils can change to a thermodynamically more stable one directly passing the barrier between two types of amyloid fibrils (route c) or indirectly through the monomers, which are in equilibrium with two types of fibrils. It is also possible that the seeding leads to the formation of fibrils with a conformation different from that of the seed fibrils (i.e., conformational adaptation during the growth of single fibrils), where seeds are used to initiate the reaction but the peptides assume a thermodynamically stable conformation (route d). Although these routes did not apply to the present results, they might come into play depending on the free energy profiles of the different conformational states. Direct and real-time observation will be important for a better understanding of the free energy diagrams of amyloid fibrils.

We would like to thank Prof. H. Naiki for his support and collaboration from the start of the project on amyloid fibrils, Prof. T. Wazawa and Dr. K. Morigaki for their technical support and discussions, and all members of our group for their contribution. This work was supported by Grants-in-Aid from the Japanese Ministry of Education, Culture, Sports, Science and Technology and by the Japan Society for Promotion of Science (JSPS) Research Fellowships for Young Scientists to T.B.

References

(1) Rochet, J. C.; Lansbury, P. T., Jr. Amyloid fibrillogenesis: themes and variations. *Curr. Opin. Struct. Biol.* **2000**, *10*, 60−68.
(2) Dobson, C. M. Protein folding and misfolding. *Nature* **2003**, *426*, 884−890.
(3) Uversky, V. N.; Fink, A. L. Conformational constraints for amyloid fibrillation: the importance of being unfolded. *Biochim. Biophys. Acta* **2004**, *1698*, 131−153.
(4) Naiki, H.; Hashimoto, N.; Suzuki, S.; Kimura, H.; Nakakiku, K.; Gejyo, F. Establishment of a kinetic model of dialysis-related amyloid fibril extension *in vitro*. *Amyloid* **1997**, *4*, 223−232.
(5) Naiki, H.; Nakakuki, K. First-order kinetic model of Alzheimer's β-amyloid fibril extension *in vitro*. *Lab. Invest.* **1996**, *74*, 374−383.
(6) Tycko, R. Insight into the amyloid folding problem from solid-state NMR. *Biochemistry* **2003**, *42*, 3151−3159.
(7) Petkova, A. T.; Leapman, R. D.; Guo, A.; Yau, W. M.; Mattson, M. P.; Tycko, R. Self-propagating, molecular-level polymorphism in Alzheimer's β-amyloid fibrils. *Science* **2005**, *307*, 262−265.
(8) Hoshino, M.; Kato, H.; Hagihara, Y.; Hasegawa, K.; Naiki, H.; Goto, Y. Mapping the core of the β_2-microglobulin amyloid fibril by H/D exchange. *Nat. Struct. Biol.* **2002**, *9*, 332−336.
(9) Whittemore, N. A.; Mishra, R.; Kheterpal, I.; Williams, A. D.; Wetzel, R.; Serpersu, E. H. (2005). H/D exchange mapping of A1-40 amyloid fibril structure using NMR spectroscopy. *Biochemistry* **2005**, *44*, 4434−4441.
(10) Dzwolak, W.; Smirnovas, V.; Jansen, R.; Winter, R. Insulin forms amyloid in a strain-dependent manner: an FT-IR spectroscopic study. *Protein Sci.* **2004**, *13*, 1927−1932.

(11) Jones, E. M.; Surewicz, W. K. Fibril conformation as the basis of species- and strain-dependent seeding specificity of mammalian prion amyloids. *Cell* **2005**, *121*, 63−72.
(12) Tanaka, M.; Chien, P.; Yonekura, K.; Weissman, J. S. Mechanism of cross-species prion transmission: an infectious conformation compatible with two highly divergent yeast prion proteins. *Cell* **2005**, *121*, 49−62.
(13) Collinge, J. Prion diseases of humans and animals: their causes and molecular basis. *Annu. Rev. Neurosci.* **2001**, *24*, 519−550.
(14) Chien, P.; Weissman, J. S.; Depace, A. H. Emerging principles of conformation-based prion inheritance. *Annu. Rev. Biochem.* **2004**, *73*, 617−656.
(15) Legname, G.; Baskakov, I. V.; Nguyen, H.-O. B.; Riesner, D.; Cohen, F. E.; DeArmond, S. J.; Prusiner, S. B. Synthetic mammalian prions. *Science* **2004**, *305*, 673−676.
(16) Gejyo, F.; Yamada, T.; Odani, S.; Nakagawa, Y.; Arakawa, M.; Kunitomo, T.; Kataoka, H.; Suzuki, M.; Hirasawa, Y.; Shirahama, T.; Cohen, A. S.; Schmid, K. A new form of amyloid protein associated with chronic hemodialysis was identified as β_2-microglobulin. *Biochem. Biophys. Res. Commun.* **1985**, *129*, 701−706.
(17) Yamamoto, S.; Gejyo, F. Historical background and clinical treatment of dialysis-related amyloidosis. *Biochim. Biophys. Acta* **2005**, *1953*, 4−10.
(18) Bjorkman, P. J.; Saper, M. A.; Samraoui, B.; Bennett, W. S.; Strominger, J. L.; Wiley, D. C. Structure of the human class I histocompatibility antigen, HLA-A2. *Nature* **1987**, *329*, 506−512.
(19) McParland, V. J.; Kalverda, A. P.; Homans, S. W.; Radford, S. E. Structural properties of an amyloid precursor of β_2-microglobulin. *Nature Struct. Biol.* **2002**, *9*, 326−331.
(20) Corazza, A.; Pettirossi, F.; Viglino, P.; Verdone, G.; Garcia, J.; Dumy, P.; Giorgetti, S.; Mangione, P.; Raimondi, S.; Stoppini, M.; Bellotti, V.; Esposito, G. Properties of some variants of human β_2-microglobulin and amyloidgenesis. *J. Biol. Chem.* **2004**, *279*, 9176−9189.
(21) Chiti, F.; Mangione, P.; Andreola, A.; Giorgetti, S.; Stefani, M.; Dobson, C. M.; Bellotti, V.; Taddei, N. Detection of two partially structured species in the folding process of the amyloidogenic protein β2-microglobulin. *J. Mol. Biol.* **2001**, *307*, 379−391.
(22) Ivanova, M. I.; Sawaya, M. R.; Gingery, M.; Attinger, A.; Eisenberg, D. An amyloid-forming segment of β_2-microglobulin suggests a molecular model for the fibril. *Proc. Natl. Acad. Sci. U.S.A.* **2004**, *101*, 10584−10589.
(23) Morgan, C. J.; Gelfand, M.; Atreya, C.; Miranker, A. D. Kidney dialysis-associated amyloidosis: a molecular role for copper in fiber formation. *J. Mol. Biol.* **2001**, *309*, 339−345.
(24) Chatani, E.; Goto, Y. Structural stability of amyloid fibrils of β2-microglobulin in comparison with its native fold. *Biochim. Biophys. Acta* **2005**, *1973*, 64−75.
(25) Ban, T.; Hamada, D.; Hasegawa, K.; Naiki, H.; Goto, Y. Direct observation of amyloid fibril growth monitored by ThT fluorescence. *J. Biol. Chem.* **2003**, *278*, 16462−16465.
(26) Ban, T.; Hoshino, M.; Takahashi, S.; Hamada, D.; Hasegawa, K.; Naiki, H.; Goto, Y. Direct observation of Aβ amyloid fibril growth and inhibition. *J. Mol. Biol.* **2004**, *344*, 757−767.
(27) Funatsu, T.; Harada, Y.; Tokunaga, M.; Saito, K.; Yanagida, T. Imaging of single fluorescent molecules and individual ATP turnovers by single myosin molecules in aqueous solution. *Nature* **1995**, *374*, 555−559.
(28) Yamasaki, R.; Hoshino, M.; Wazawa, T.; Ishii, Y.; Yanagida, T.; Kawata, Y.; Higurashi, T.; Sakai, K.; Nagai, J.; Goto, Y. Single molecular observation of the interaction of GroEL with substrate proteins. *J. Mol. Biol.* **1999**, *292*, 965−972.
(29) Wazawa, T.; Ueda, M. Total internal reflection fluorescence microscopy in single molecule nanobioscience. *Adv. Biochem. Eng. Biotechonol.* **2005**, *95*, 77−106.
(30) Naiki, H.; Higuchi, K.; Hosokawa, M.; Takeda, T. Fluorometric determination of amyloid fibrils *in vitro* using the fluorescent dye, thioflavin T. *Anal. Biochem.* **1989**, *177*, 244−249.
(31) Hoyer, W.; Cherny, D.; Subramaniam, V.; Jovin, T. M. Rapid self-assembly of α-synuclein observed by *in situ* atomic force microscopy. *J. Mol. Biol.* **2004**, *340*, 127−139.
(32) Kad, N. M.; Myers, S. L.; Smith, D. P.; Smitj, D. A.; Radford, S. E.; Thomson, N. H. Hierarchical assembly of β_2-microglobulin amyloid *in vitro* revealed by atomic force microscopy. *J. Mol. Biol.* **2003**, *330*, 785−797.
(33) Ohhashi, Y.; Kihara, M.; Naiki, H.; Goto, Y. Ultrasonication-induced amyloid fibril formation of β2-microglobulin. *J. Biol. Chem.* **2005**, *280*, 32843−32848.
(34) MacPhee, C. E.; Dobson, C. M. Chemical dissection and reassembly of amyloid fibrils formed by a peptide fragment of trysthyretin. *J. Mol. Biol.* **2000**, *297*, 1203−1215.
(35) Kozhukh, G. V.; Hagihara, Y.; Kawakami, T.; Hasegawa, K.; Naiki, H.; Goto, Y. Investigation of a peptide responsible for amyloid fibril formation of β_2-microglobulin by achromobacter protease I. *J. Biol. Chem.* **2002**, *277*, 1310−1315.
(36) Ohhashi, Y.; Hasegawa, K.; Naiki, H.; Goto, Y. Optimum amyloid fibril formation of a peptide fragment suggests the amyloidogenic preference of β_2-microglobulin under physiological conditions. *J. Biol. Chem.* **2004**, *279*, 10814−10821.
(37) Chiti, F.; Bucciantini, M.; Capanni, C.; Taddei, N.; Dobson, C. M.; Stefani, M. Solution conditions can promote formation of either amyloid protofilaments or mature fibrils from HypF N-terminal domain. *Protein Sci.* **2001**, *10*, 2541−2547.
(38) Li, H.-T.; Du, H.-N.; Tang, L.; Hu, J.; Hu, H.-Y. Structural transformation and aggregation of human alpha-synuclein in trifluoroethanol. *Biopolymers* **2002**, *64*, 221−226.
(39) Wadai, H.; Yamaguchi, K.; Takahashi, S.; Kanno, T.; Kawai, T.; Naiki, H.; Goto, Y. Stereospecific amyloid-like fibril formation by a peptide fragment of β_2-microglobulin. *Biochemistry* **2005**, *44*, 157−164.
(40) Yamaguchi, K.; Takahashi, S.; Kawai, T.; Naiki, H.; Goto, Y. Seeding-dependent propagation versus maturation of amyloid fibril conformation. *J. Mol. Biol.* **2005**, *352*, 952−960.
(41) Kihara, M.; Chatani, E.; Sakai, M.; Hasegawa, K.; Naiki, H.; Goto, Y. Seeding-dependent maturation of β_2-microglobulin amyloid fibrils at neutral pH. *J. Biol. Chem.* **2005**, *280*, 12012−12018.
(42) Kraulis, P. J. MOLSCRIPT: a program to produce both detailed and schematic plots of protein structures. *J. Appl. Crystallogr.* **1991**, *24*, 946−950.

AR050074L